Theoretical Modeling of the Hydrogen Abstraction Reaction of Fluoromethane by the Hydroxyl Radical†

Pei-Yin Lien, Ru-Min You, and Wei-Ping Hu*

Department of Chemistry, National Chung Cheng University, Chia-Yi, Taiwan 621, ROC

Received: September 13, 2000; In Final Form: December 1, 2000

We have performed theoretical modeling of the reaction rate constants of the hydrogen abstraction reaction of fluoromethane (CH_3F) by the hydroxyl radical (OH) using dual-level variational transition state theory calculation including multidimensional tunneling corrections from 200 to 1000 K. Correlated electronic structure theory with extended basis set calculation was applied for both the low-level reaction-path and the high-level stationary-point calculation. An improved interpolated correction scheme was used for better estimating the width of energy barrier by performing an intermediate-level electronic structure calculation. The calculated rate constants are in good agreement with available experimental values at most temperatures. The hydrogen kinetic isotope effects (KIEs) were also evaluated and analyzed. The current study suggested that the reaction has a relatively wide barrier, and the tunneling effects are thus not very important even at low temperatures. The current study also showed that the variational effects, which lowered the rate constants by over an order of magnitude at room temperature, are very important for the reaction. The best estimate of the classical barrier height is between 2.8 and 3.1 kcal/mol. The calculation also suggested that the calculated KIEs are sensitive to the theories employed for obtaining the low-level potential energy surfaces. It is demonstrated that the dynamical behaviors predicted by the current calculation can also be deduced from future KIE experiments on the current reaction.

Introduction

The atmospheric chemistry of the hydrofluorocarbons (HFCs) has been extensively studied in recent years.[1−13] This is mainly because the HFCs have been proposed and utilized as substitutes for the industrial and household uses of chlorofluorocarbons (CFCs), which are believed to have caused the ozone depletion in the stratosphere. One of the reasons that HFCs are more ozone-friendly is that they contain C−H bonds that are susceptible to attack by hydroxyl radicals that are abundant in the atmosphere, e.g.,

$$OH + CH_3F \rightarrow H_2O + CH_2F \qquad (R1)$$

As a consequence, the HFCs' atmospheric lifetime[1,9] is much shorter than that of CFCs. Despite being ozone-friendly, the HFCs, however, are potential greenhouse gases and absorb infrared radiation not absorbed by carbon dioxide and water vapor.[9] Thus, it is important, from the experimental point of view, to measure exactly how fast the HFCs are consumed in the atmosphere and, from the theoretical point of view, to understand the detailed physical properties of the main HFCs removing reactions.

There have been many experimental studies on (R1), the gas-phase reaction between the simplest HFC and the hydroxyl radical. The experimental techniques used include discharge flow systems,[4,6a] flash-photolysis methods,[5,9] and relative rate measurements.[10,11] Generally speaking, rate constants obtained by flow tube methods are lower than those measured by flash-photolysis methods, especially at lower temperatures.[9] As early as in 1976, Howard and Evenson[4] measured the rate constant of (R1) at 296 K using a discharge flow system. Nip et al.[5] in 1979 obtained the rate constant at 297 K using the flash-photolysis technique. Then in 1982 Jeong and Kaufman[6a] measured the rate constants in the temperature range of 292−480 K using a discharge flow system. The above experimental results were compiled in 1985 by Atkinson,[7] and his recommended expression for rate constants from 292 to 480 K was

$$k = 5.51 \times 10^{-18} T^2 \exp(-1005 \pm 168/T) \text{ cm}^3 \text{ molecule}^{-1} \text{ s}^{-1} \quad (1)$$

Schmoltner et al.[9] in 1993 measured the rate constants of (R1) from 243 to 373 K with the pulsed laser photolysis technique and fitted the results to the following Arrhenius expression:

$$k = 1.75 \times 10^{-12} \exp(-1300/T) \text{ cm}^3 \text{ molecule}^{-1} \text{ s}^{-1} \quad (2)$$

Their results are in good agreement with Nip et al.'s value at 297 K but are slightly higher than Jeong and Kaufman's values. This is also the only experiment that extended the temperature range below 296 K. However, the results showed relatively large uncertainty at the lowest temperatures. Hsu and DeMore[10] studied (R1) with the relative rate methods from 298 to 363 K in 1995 with HFC-152a as the reference, and then in 1996 DeMore[11] remeasured the rate constants from 308 to 393 K with reference to CH_3Cl. Combining the two relative rate measurements, DeMore[11] fitted the rate constants with the following Arrhenius expression:

$$k = 4.4 \times 10^{-12} \exp(-1655/T) \text{ cm}^3 \text{ molecule}^{-1} \text{ s}^{-1} \quad (3)$$

These results are in good agreement with Schmoltner et al.'s

† Part of the special issue "Aron Kuppermann Festschrift".

* To whom correspondence should be addressed. E-mail: chewph@ccunix.ccu.edu.twFax: 886-5-272-1040.

10.1021/jp003260b CCC: $20.00
Published on Web 02/20/2001

values in the upper-temperature range. All the experimental data covering a temperature range showed very little, if any, curvature in the Arrhenius plot.[6a,7,9−11]

There have also been several theoretical studies on (R1) in recent years. Jeong and Kaufman[6b] applied conventional transition state theory (CTST or TST)[14,15] in 1982 to calculate the Arrhenius preexponential factor of the reaction. They also used Wigner's formula[16,17] and Eckart potential transmission coefficients[18] to estimate the tunneling correction. Cohen and Benson[8] carried out more detailed theoretical study on the reactions of OH with different haloalkanes in 1987 based also on TST, although the possible application of variational transition state theory (VTST)[15,17] was briefly mentioned. In 1998 Schwartz et al.[12] made a high-level computational study on the hydrogen abstraction reactions of different fluoromethanes by OH. The reaction rate constants were modeled by TST and an improved tunneling correcting method based on Eckart potential functions. Good agreement with available experimental data was obtained. However, it is now known that the variational effects can sometimes affect the reaction rate constants significantly,[15,17,19−23] especially for low-barrier reactions. Also, the simple and popular one-dimensional tunneling approximations may sometimes severely underestimate the extent of tunneling.[15,17,27] To accurately model the reaction rate constants and study various dynamical properties of a reaction, the variational effects and multidimensional tunneling (MT)[15,17,24−27] need to be taken into account.

Also in 1998, Espinosa-Garcia et al.[13] studied (R1) by applying dual-level VTST calculation including multidimensional tunneling corrections. It is puzzling, however, that the calculated Arrhenius plot showed significant curvature at lower temperatures, which seemed to be inconsistent with the low-temperature data of Schmoltner et al.[9] and Hsu and DeMore.[10,11] As a matter of fact, the Arrhenius plots of the hydrogen abstraction reaction of all fluoromethanes (CH_3F, CH_2F_2, and CHF_3) by OH show very little curvature.[7,9−11] Since the VTST/MT methods have been proved to be able to accurately model the reaction rate constants over extended temperature range,[19−21,28−32] we suspect that the PM3[33] semiempirical method employed to calculate the low-level potential energy surface (PES) in ref 13 might not be sufficiently accurate, and this in turn caused the discrepancy with experimental data at lower temperatures.

In the current study we applied the dual-level[23,28,29] VTST/MT dynamics method to model the reaction rate constants of (R1) by using a much more accurate electronic structure theory to obtain the underlying low-level PES information. We used one of our newly developed improved interpolated correction schemes[23] (SIL-2) to carry out the low-level to high-level PES data correction.[28] In essence, the new correction scheme incorporates data from an intermediate-level classical (or Born−Oppenheimer) energy calculation along the reaction path to better estimate the width of the reaction energy barrier. In doing so, we ensured that not only a qualitatively correct low-level PES was used but also more reliable tunneling corrections were calculated. We also calculated the rate constants of the isotopic analogue of (R1):

$$OH + CD_3F \rightarrow HDO + CD_2F \qquad (R2)$$

We will show that by studying the kinetic isotope effects (KIEs, k_1/k_2) and their temperature dependence experimentally, various dynamical properties of the current reaction, such as the barrier height, the variational effects, and the tunneling effects, can be probed.

Method

Molecular geometry optimization and vibrational frequencies of the stationary points were calculated using AM1[34] and PM3 semiempirical methods (in which the various two- and one-electron integrals were either omitted or were approximated using parameter sets), the full Hartree−Fock[35] (HF) theory with 6-31+G** and 6-311+G** basis sets,[36] and Møller−Plesset second-order perturbation theory[37](MP2) with 4-31G*,[36] 6-31+G**, and 6-311+G** basis sets. Born−Oppenheimer energies of reaction and barrier heights were also calculated using the quadratic configuration interaction theory including single and double substitutions with the triples contribution added pertubatively[38] [QCISD(T)] with 6-311+G** and 6-311++G(3df,3pd) basis sets at the MP2/6-31+G** and MP2/6-311+G** optimized geometry.

Dual-level VTST calculation with the SIL-2 correction scheme[23] requires three levels of electronic structure calculation, including the low-level reaction-path calculation, the intermediate-level barrier-width estimation, and the high-level stationary-point calculation. The low-level calculation includes the geometry, energies, gradients, and vibrational normal-modes computation along the reaction path. The low-level theory used in the current study is MP2/6-31+G**. The symmetry number for the reaction is set to three. The scaled mass was set to 1 amu and the reaction path was calculated using the Page−McIver method[39] from −2.0 to +0.8 bohrs for (R1) and −1.7 to +0.5 bohrs for (R2) with gradient and Hessian step sizes of 0.005 and 0.025 bohrs, respectively. The redundant internal coordinates[40] were used for the vibrational analysis of the generalized transition states. The intermediate-level calculation involves computing the classical energy along the reaction path. The SIL schemes[23] are flexible about the levels of calculation used for the intermediate level. A convenient choice is using the reaction-path geometry obtained from the low-level calculation to perform higher level single-point energy calculation. In the current study we used QCISD(T)/6-311+G** method to obtain the required intermediate-level energy profile along the low-level reaction-path geometry, and estimated the half-height width of the barrier ($s_{1/2}$).[23] The high-level calculation includes geometry and frequency computation of the reactants, transition state, and products. This was carried out at the MP2/6-311+G** level, as mentioned at the beginning of this section. The high-level energy of reaction is taken as the experimental value of −15.4 kcal/mol.[41] A summary to the levels of the electronic theory mentioned above is the following: The MP2/6-31+G** level was used as the low-level theory to obtain the underlying global PES information, including the energies, molecular geometry, and vibrational frequencies. The calculated results form the basis for the subsequent dual-level interpolated correction. To facilitate the SIL-2 correction scheme, an intermediate-level single-point calculation at QCISD(T)/6-311+G** level was performed along the reaction-path geometry calculated at the low-level theory. This calculation gave the estimated width of the classical energy barrier that was then used in the subsequent dual-level correction to derive the range parameter of the correction function. The geometry optimization and vibrational frequency calculation was also performed at the MP2/6-311+G** level to obtain more accurate molecular geometry and harmonic frequencies of the stationary points. These data were used as the high-level geometry and frequency values in the dual-level calculation. Even though it seems that the MP2/6-311+G** is a lower level theory than the intermediate level, the analytical first and second derivatives of the QCISD(T) method are not currently available, and thus it and

other sophisticated electronic theories, such as MP4(SDTQ) and CCSD(T), are not suitable for geometry optimization and frequency calculation.

The dual-level reaction rate constants were calculated using the conventional transition state theory (TST) and the canonical variational theory (CVT).[15,17] The tunneling correction was evaluated using the microcanonical optimized multidimensional tunneling (μOMT)[26,27] approximation that takes the dominant tunneling probability calculated with the small- and large-curvature tunneling (SCT[25] and LCT[17,24,26]) approximation at a given energy. The vibrational partition functions were calculated using the harmonic approximation except for the lowest-frequency hindered rotor mode (mode 13 at MP2/6-31+G** level and mode 14 at MP2/6-311+G** level) of the transition state and the generalized transition states. We applied the ωW scheme developed by Truhlar et al.[42] to calculate the vibrational partition function of that mode. The ICL method[43] was used in the dual-level frequency correction. In the LCT calculation, only the product ground state was considered, and the linear method[23,28] was used for the potential energy correction in the nonadiabatic regions.[24−26]

For most polyatomic reactions, accurately calculating the classical barrier heights to chemical accuracy is still a very difficult task. Unfortunately, the reaction rate constants are extremely sensitive to the numerical value of the barrier height. Thus, instead of using the calculated barrier height directly, for accurate modeling of the reaction rate constants, we chose to take the classical barrier height as an adjustable parameter to fit to the experimental data. Most of the experimental rate constants agree within experimental errors with each other at temperature above 350 K, but some of the values obtained by Schmoltner et al.[9] at lower temperature are significantly higher. It is unclear which sets of data are more accurate. We chose to adjust the classical barrier height to fit the calculated CVT/μOMT rate constant to the experimental value as obtained from eq 3 at 350 K (3.89×10^{-14} cm^3 molecule^{-1} s^{-1}) and to the value from eq 2 at 250 K (9.65×10^{-15} cm^3 molecule^{-1} s^{-1}). The resulting barrier heights are very close to each other. See the next section for more discussion.

In the current study we also made a modification to our SIL-2 correction scheme.[23] One important but somewhat bold assumption made in the original SIL-2 scheme is

$$\mathrm{ZPE}^{\mathrm{GT}}_{\mathrm{HL}}(s_{1/2}) = \mathrm{ZPE}^{\mathrm{GT}}_{\mathrm{LL}}(s_{1/2}) + {}^1/_2\,\Delta \qquad (4)$$

That is, we assumed that the correction to the low-level vibrational zero-point energy at $s = s_{1/2}$ is equal to the average of the corrections at the reactants and at the transition state, where s is the mass-scaled reaction coordinate. In this study, we decided to put this approximation to a test, and we also used an alternative approach to estimate the high-level zero-point energy at $s = s_{1/2}$. We reasoned that if one can afford to calculate the high-level frequencies at the three stationary points, one probably can also afford to calculate the zero-point energy with the same level of theory at $s = s_{1/2}$. As a consequence, one can replace the approximation in eq 4 with the directly calculated high-level value. Of course, considerable amount of additional computation is required to follow the reaction-path from the saddle point ($s = 0$) to $s = s_{1/2}$ at the theoretical level of the high-level frequency calculation. However, gradient-based (first-order) methods,[44] which are much less resource-demanding than the Hessian-based (second-order) methods, can be used to calculate the reaction path, and the expensive vibrational analysis is only needed at $s = s_{1/2}$. We call this new approach the SIL-2-direct method. In the current study, we used Euler's method[44] to calculate the reaction-path from the saddle point to $s = s_{1/2}$ with a gradient step size of 0.005 bohr, and the Hessians were only evaluated at $s = s_{1/2}$. The results are discussed in the next section.

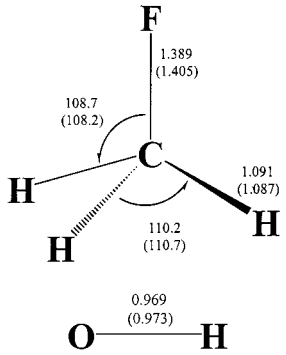

Figure 1. Calculated reactant geometry at the MP2/6-311+G** level. The bond lengths are in angstroms, and bond angles in degrees. The values in parentheses are the MP2/6-31+G** results.

To study how different low-level PES affect the dual-level dynamics calculation, we have also used the PM3 method as the low-level theory, and with the same high-level geometry, frequency, and energy of reaction information described above to performed dual-level rate constant calculation using the traditional SECKART correction scheme.[23,28] The low-level reaction path was calculated from -1.5 to $+1.0$ bohr, and all other parameters and options were identical to the calculation described above. The high-level barrier was determined by fitting the calculated CVT/μOMT rate constants to the value of eq 3 at 350 K. In fact, we have tried to use PM3 and MP2/4-31G* methods as the low-level theory and to apply the SIL-2 correction scheme. However, the classical energy profiles along the reaction path calculated by these two methods are very different from those obtained at higher levels of theory. As a result, appropriate range parameters could not be found to perform the SIL-2 correction.[23] See more detailed discussion in the next section.

In the current study, the electronic structure calculation was performed using the Gaussian 98 program,[36] and the dual-level direct dynamics calculation was carried out using the Gaussrate 8.2 program,[45] which provides an interface between the Gaussian 98 and the Polyrate 8.2 VTST/MT program.[46] The above calculation was carried on several PC workstations running Red Hat Linux, an SGI Octane workstation in our group, and on an Origin 2000 sever in the National Center for High-Performance Computing in Taiwan.

Results and Discussion

Geometry. Figures 1−3 show the calculated molecular geometry of the reactants, products, and the transition state (TS), respectively, at the MP2/6-31+G** and MP2/6-311+G** levels. It is seen in these figures that the geometry calculated by the two methods is very similar, with the differences in bond length within 0.02 Å (including the bond being broken and the bond being formed in the TS) and the bond angle differences within 2°. The calculated CH_3F geometry is in good agreement with the experimental C−F bond length of 1.391 ± 0.005 Å, C−H bond length of 1.095 ± 0.010 Å, and H−C−H bond angle of 109.5 ± 2°.[47] All the calculated geometry parameters are very similar to the MP2(Full)/6-31G** and ROMP2/6-311G-(2d,2p) results in ref 13 except for the C−H3−O angle in the TS where our MP2/6-311+G** value is 6.7° larger than the ROMP2 value. The calculated C−H3 bond length in the TS is

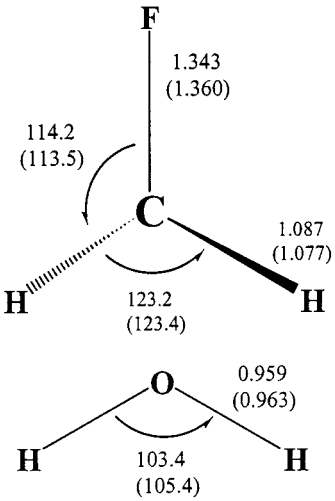

Figure 2. Calculated product geometry at the MP2/6-311+G** level. The bond lengths are in angstroms and bond angles in degrees. The values in parentheses are the MP2/6-31+G** results. The dihedral angle $D_{H-C-F-H} = 148.5°$ (143.9°).

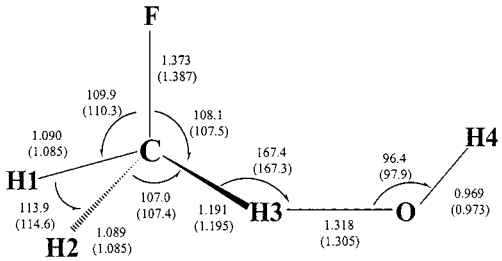

Figure 3. Calculated transition state geometry at the MP2/6-311+G** level. The bond lengths are in angstroms and bond angles in degrees. The values in parentheses are the MP2/6-31+G** results.

TABLE 1: Calculated Born−Oppenheimer Energies of Reaction and Barrier Heights (kcal/mol) of (R1) at Various Levels

	E_{rxn}	$\Delta V^{\neq}$
AM1	−31.08	8.56
PM3	−24.07	8.24
HF/6-31+G**	−2.51	27.59
HF/6-311+G**	−2.96	27.25
MP2/4-31G*	−11.27	11.70
MP2/6-31+G**	−16.50	10.04
MP2/6-311+G**	−18.36	8.97
QCISD(T)/6-311+G**//MP2/6-31+G**	−14.27	6.55
QCISD(T)/6-311+G**//MP2/6-311+G**	−14.35	6.51
CCSD(T)/aug-cc-pVTZ//MP2/6-31G** [a]	−15.6	5.1
QCISD(T)/6-311++G(3df,3pd)//MP2/6-311+G**	−16.47	4.37
best estimate[b]		2.80−3.06
expt[c]	−15.4 ± 2	

[a] From ref 13. [b] Values obtained by fitting to experimental values, See text. [c] ΔH_f(298 K) from ref 41 and zero-point and thermal energy correction from MP2/6-311+G** calculation.

only about 0.1 Å longer than that in the reactant, and thus the TS is a typical "early" transition state.

Energetics and Barrier Heights. Table 1 lists the calculated Born−Oppenheimer energies of reaction and barrier heights at various levels. The derived experimental value of reaction energy[41] is also included. The two semiempirical methods significantly overestimate the reaction exoergicity by 9−12 kcal/mol, while the Hartree−Fock method underestimates the exoergicity by 12−13 kcal/mol. There is, however, some uncertainty[13] on the experimental heat of formation of CH_3F and thus on the energy of reaction. The MP2 calculation gives results much closer to the experimental value currently used. The quality of the basis sets makes more differences in the MP2 calculation than in the HF calculation. Single-point calculation at the QCISD(T) with 6-311+G** and 6-311++G(3df,3pd) basis sets and the CCSD(T)/aug-cc-pVTZ calculation[13] all produce values very close to the experimental energy of reaction. The calculated classical barrier heights range from 4.4 kcal/mol at QCISD(T)/6-311++G(3df,3pd) level and 5.1 kcal/mol at CCSD(T) level of ref 13 to 27.6 kcal/mol at HF/6-31+G** level. Our best estimate of the classical barrier height by fitting to the experimental rate constants is 2.8−3.1 kcal/mol. This will be further discussed later in this section.

TABLE 2: Calculated Stationary-Point Vibrational Frequencies (cm^{-1}) of (R1) at the MP2/6-311+G Level**

CH_3F	OH	CH_2F	H_2O	TS
3197.3	3835.9	3357.0	4002.4	3830.6
3197.3		3195.6	3884.2	3237.0
3093.2		1503.7	1629.6	3134.5
1522.2		1202.1		1531.4
1522.2		1182.8		1497.1
1517.4		702.1		1320.6
1216.6				1264.7
1216.6				1189.9
1076.6				1111.2
				869.2
				742.7
				302.9
				121.2
				111.6
				1953.8i

TABLE 3: Calculated Stationary-Point Vibrational Frequencies (cm^{-1}) of (R2) at the MP2/6-311+G Level**

CD_3F	OH	CD_2F	HDO	TS
2375.3	3835.9	2512.4	3945.9	3830.5
2375.3		2302.9	2864.2	2410.7
2213.2		1220.6	1428.2	2269.8
1177.7		1044.1		1194.1
1102.9		921.0		1108.0
1102.9		552.1		1045.3
1012.3				989.0
933.2				940.5
933.2				927.0
				797.3
				705.4
				225.4
				117.6
				108.5
				1443.5i

Vibrational Frequencies and Zero-Point Energies. The calculated harmonic vibrational frequencies of the stationary points of (R1) and (R2) at MP2/6-311+G** level are listed in Tables 2 and 3, respectively. The frequencies calculated at the MP2/6-31+G** level are included in the Supporting Information. It is clearly seen that one of the high-frequency C−H (C−D) stretching modes in CH_3F (CD_3F) disappears in the transition state. This mode corresponds to the hydrogen abstracted by the OH radical, and it contributes strongly to the kinetic isotope effects calculated by TST, as will be discussed later in this section. The vibrational zero-point energy (ZPE) at $s = s_{1/2}$ calculated by the SIL-2-direct method is 31.98 kcal/mol and is only 0.16 kcal/mol lower than the value estimated by eq 4 using the original SIL-2 method.[23] That is, the approximation in the original SIL-2 scheme is actually quite good. To test the accuracy of the SIL-2-direct approach, which uses the gradient-based Euler method to calculate the MP2/6-311+G** reaction-path geometry, we also used the probably more accurate Hessian-based Page−McIver method to calculate

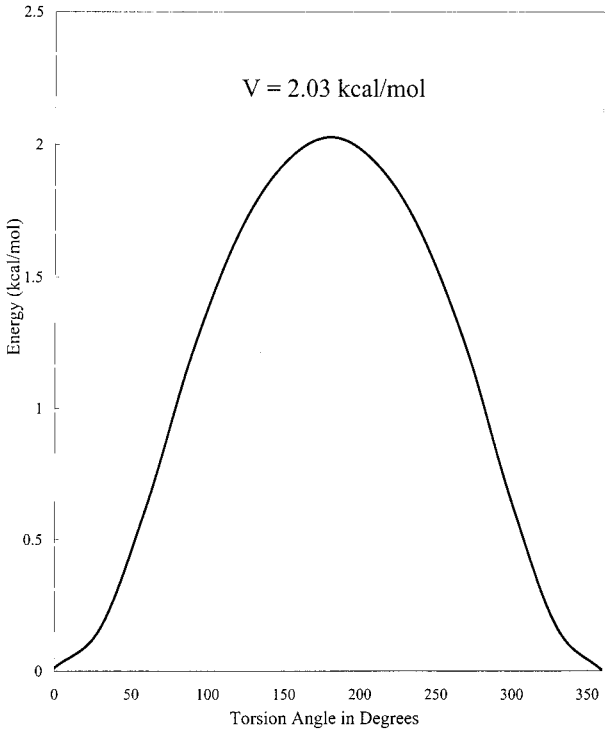

Figure 4. Calculated classical energy profile along the torsion angles for the hindered rotor mode at MP2/6-311+G** level.

the MP2/6-311+G** reaction path from the saddle point to $s = s_{1/2}$ using the same parameters as in the low-level (MP2/6-31+G**) reaction-path calculation. The calculated ZPE at $s = s_{1/2}$ is within 0.001 kcal/mol of the value obtained by the SIL-2-direct approach. To make the calculation less resource demanding, we also tried doubling the Hessian step size for the Page−McIver method and the resulting ZPE values are identical. However, calculating this higher-level reaction path using Hessian-based methods is extremely time-consuming and is not recommended for general uses. The above calculation showed when the necessary computational resource is available, the SIL-2-direct approach can be applied to better estimate the ZPE at $s = s_{1/2}$ by using a gradient-based method to calculate the required range of the reaction-path at a higher level of theory. For more complex chemical systems, however, the original SIL-2 scheme is still recommended for resource consideration.

As mentioned in the previous section, the lowest-frequency (111.6 cm^{-1}) mode of the transition state is treated as a hindered rotor using the ωW scheme. This involves estimating the rotational barrier.[42] We approximated the rotational coordinate as the C−H3−O−H4 (see Figure 3) dihedral angle. The potential energy profile along the rotational coordinate was calculated (with all atoms fixed except H4) at MP2/6-311+G** level, and it is plotted in Figure 4. As shown in the figure, there is only one energy maximum and the rotational barrier is estimated to be 2.03 kcal/mol.

Rate Constants. The calculated bimolecular rate constants of (R1) at various temperatures are listed in Table 4 along with two sets of experimental data by DeMore[11] and Schmoltner et al.[9] Two sets of calculated rate constants are listed, as mentioned in the previous section, one set was fitted to DeMore's data at 350 K and the other set was fitted to Schmoltner et al.'s data at 250 K with adjusted classical barrier heights of 3.06 and 2.80 kcal/mol, respectively. This is compared to the estimated values of 5.1 kcal/mol by Schwartz et al.[12] and 5.2 kcal/mol by Espinosa-Garcia et al.[13] For comparison purpose, we also calculated the rate constants using the high-level classical barrier

TABLE 4: Calculated Dual-Level Rate Constants (cm^3 $molecule^{-1}$ s^{-1}) of (R1) Using MP2/6-31+G as the Low-Level Theory**

T (K)	TST	CVT	CVT/μOMT	expt[a]	expt[b]
200	6.42(−14)[c]	1.23(−15)	1.71(−15)		
	1.23(−13)[d]	2.18(−15)	2.56(−15)		
250	1.32(−13)	5.60(−15)	6.82(−15)		9.65(−15)
	2.21(−13)	8.87(−15).	9.65(−15)		
300	2.23(−13)	1.61(−14)	1.83(−14)	1.77(−14)	2.30(−14)
	3.44(−13)	2.36(−14)	2.48(−14)		
350	3.40(−13)	3.54(−14)	3.89(−14)	3.89(−14)	4.27(−14)
	4.93(−13)	4.92(−14)	5.07(−14)		
400	4.85(−13)	6.58(−14)	7.06(−14)	7.02(−14)	
	6.70(−13)	8.81(−14)	8.95(−14)		
450	6.59(−13)	1.09(−13)	1.15(−13)		
	8.79(−13)	1.42(−13)	1.43(−13)		
500	8.66(−13)	1.68(−13)	1.75(−13)		
	1.12(−12)	2.12(−13)	2.13(−13)		
600	1.39(−12)	3.34(−13)	3.43(−13)		
	1.73(−12)	4.06(−13)	4.05(−13)		
800	2.99(−12)	8.97(−13)	9.05(−13)		
	3.51(−12)	1.04(−12)	1.03(−13)		
1000	5.46(−12)	1.81(−12)	1.82(−12)		
	6.22(−12)	2.04(−12)	2.01(−12)		

[a] From DeMore's Arrehenius expression.[11] [b] From Schmolter et al.'s Arrehenius expression.[9] [c] 6.42(−14) means 6.42×10^{-14} [d] Upper values are results fitted to experimental rate constants of ref 11 at 350 K, and the lower values are results fitted to experimental rate constants of ref 9 at 250 K. See text.

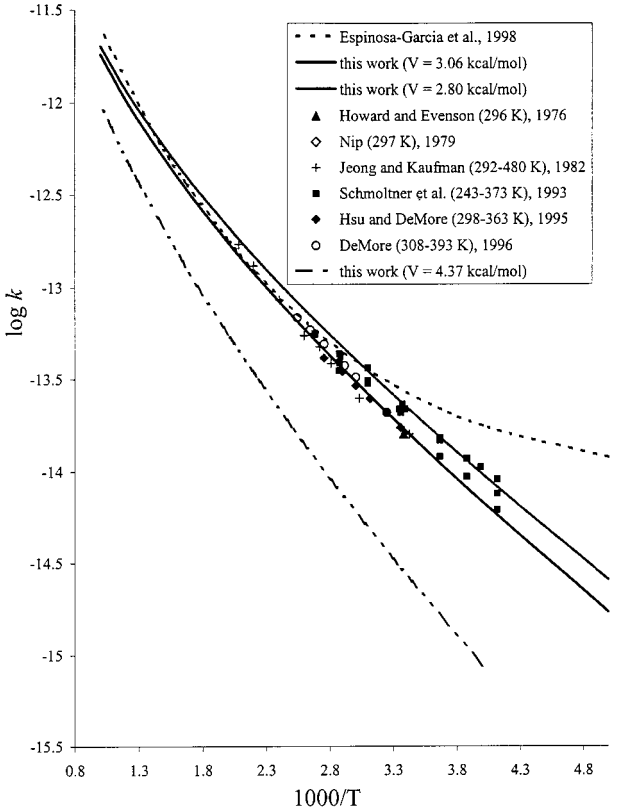

Figure 5. Arrhenius plot of the experimental and calculated rate constants (in cm^3 $molecule^{-1}$ s^{-1}) of (R1).

of 4.37 kcal/mol obtained at the QCISD(T)/6-311++G(3df,-3pd)//MP2/6-311+G** level. The Arrhenius plot of the calculated and experimental rate constants of (R1) is shown in Figure 5, and the results of Espinosa-Garcia et al.[13] are also included. The lowest curve corresponds to the values calculated with a classical barrier of 4.37 kcal/mol. All the calculated rate constants are well below the experimental data. (The numeric values of the calculated rate constants are included in the

TABLE 5: Percentage Decrease of the Classical Energies along the Reaction Path Relative to the Classical Barrier Height at Various Levels

s (bohrs)	MP2/6-311+G**	MP2/6-31+G**	MP2/4-31G*	PM3
0	0.0%	0.0%	0.0%	0.0%
−0.05	1.0%	1.1%	1.3%	2.0%
−0.10	3.4%	3.7%	4.8%	7.1%
−0.15	6.0%	6.7%	9.3%	13.7%
−0.20	8.7%	9.6%	14.0%	20.7%
−0.25	11.3%	12.4%	18.4%	27.1%
−0.30	14.0%	15.2%	22.4%	33.0%
−0.35	16.7%	18.0%	26.0%	38.6%
−0.40	19.4%	20.8%	29.5%	44.1%
−0.45	22.1%	23.5%	32.9%	49.4%
−0.50	24.7%	26.3%	36.2%	54.7%
−0.55	27.4%	29.0%	39.4%	59.8%
−0.60	30.0%	31.7%	42.5%	64.8%

Supporting Information.) For example, at 300 K, the calculated rate constant is about 6−7 times smaller than the experimental values. The second lowest curve ($V^{\neq} = 3.06$ kcal/mol) fits all experimental data well except in the lowest temperature range. The next curve ($V^{\neq} = 2.80$ kcal/mol) on the other hand fits most of the Schmoltner et al.'s and Nip's[5] values well and is only slightly higher than the lowest curve at higher temperatures. Future experiments, especially at lower temperatures, might be necessary to resolve the discrepancy and uncertainty of the low-temperature rate constants. Our calculation shows, in contrast to ref 13, only very little curvature in the Arrhenius plot, which seems to be more consistent with recent experimental results. In the current study, the dominant tunneling mechanism is the small-curvature tunneling in the dual-level calculation. As seen in Table 4, the tunneling effects raise the CVT rate constants by only 5−14% at 300 K. The lack of curvature or the tunneling effects is due to the low and wide energy barrier of the reaction. This has also been suggested by Schwartz et al.[12] However, the large variational effects (the differences between the TST and CVT rate constants), as shown in Table 4, have not been considered in previous TST studies. At 300 K, the variational effects lower the calculated rate constants by over an order of magnitude. The variational effects are less dramatic for (R2). (See the Supporting Information for the calculated (R2) rate constants.)

We have mentioned in previous sections that the choices of low-level PES may have profound effects on the calculated dual-level rate constants. In Table 5 we listed the ratios of the energy decrease relative to the classical barrier height along the reactant-side reaction path at four different theoretical levels. The corresponding classical energy profiles are plotted in Figure 6. It is clearly seen that the energies calculated at the MP2/4-31G* and PM3 levels decrease much faster than those calculated at the other two levels. For example, from the saddle point ($s = 0.0$) to $s = -0.5$ bohr, the MP2/4-31G* and PM3 energies have decreased by 36% and 55%, respectively, while the MP2/6-311+G** and MP2/6-31+G** energies have only decreased by 25% and 26%, respectively. Except for the absolute values, the overall shapes of the energy profiles calculated at the MP2/6-311+G** and MP2/6-31+G** levels are very similar. When we tried to use either PM3 or MP2/4-31G* as our low-level theory for dual-level dynamics calculation, suitable range parameters[23] cannot be found to perform the SIL-2 correction scheme because the energy profiles calculated at these levels are qualitatively different from those calculated at higher theoretical levels. Thus, in the current theoretical modeling, the more reliable MP2/6-31+G** method was used for the low-level reaction-path calculation. The dual-level calculation using the PM3 as the low-level theory was performed only for comparison purposes, as will be discussed shortly in this section. The dual-level vibrationally adiabatic ground-state energy (classical energy plus ZPE) curves along the reaction path (V_a^G) are plotted in Figure 7. It is seen that the maxima of the curves are shifted toward the reactant side and are significantly higher (>1 kcal/mol) than the values at the saddle point. Thus, the calculated rate constants show large variational effects. The curve using the MP2/6-31+G** method as the low level shows a very wide barrier, whereas the one using the PM3 method as the low level has a much narrower barrier. The excessive tunneling effects calculated in ref 13, as seen in Figure 5, are probably due to the erroneously narrow width of the energy barrier predicted by the PM3 method.

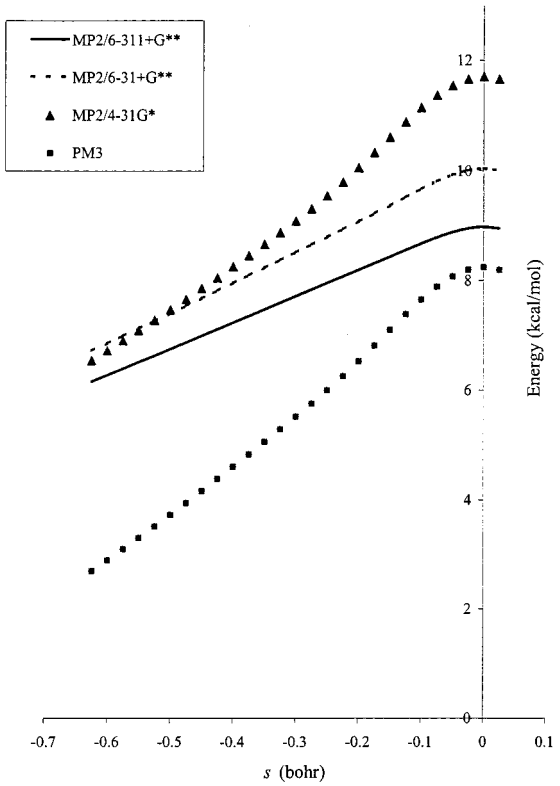

Figure 6. Born-Oppenheimer energy profiles along the R1 reaction path (V_{MEP}) on the reactant side calculated at different levels.

Kinetic Isotope Effects. The calculated KIEs using the two fitted classical barrier heights mentioned above are shown in Table 6. We also include the KIEs calculated using the PM3 method as the low-level PES. In that calculation the high-level classical barrier height (4.58 kcal/mol) was fitted to reproduce the DeMore's[11] experimental value at 350 K. It is noted in Table 6 that the KIEs calculated by TST are much larger than the CVT values. For the calculation using the MP2/6-31+G** as the low-level PES, tunneling effects make the KIEs slightly smaller. For example, at 300 K the high-level TST predicted a KIE of 7.40, while the CVT and CVT/μOMT predicted 1.60 and 1.57, respectively, for the calculation using 3.06 kcal/mol as the classical barrier height. In fact, the two calculations using the MP2/6-31+G** theory as the low-level PES produced very similar KIEs. However, the calculation using the PM3 method as the low-level PES gave very different results. As shown in Table 6, the KIEs calculated by CVT are close to unity and are significantly smaller than those calculated using the MP2/6-31+G** as the low-level PES. When tunneling effects are considered, the calculation using the PM3 as the low-level PES showed significant normal KIEs at low temperatures. For example, at 300 K the KIEs calculated by CVT and CVT/μOMT

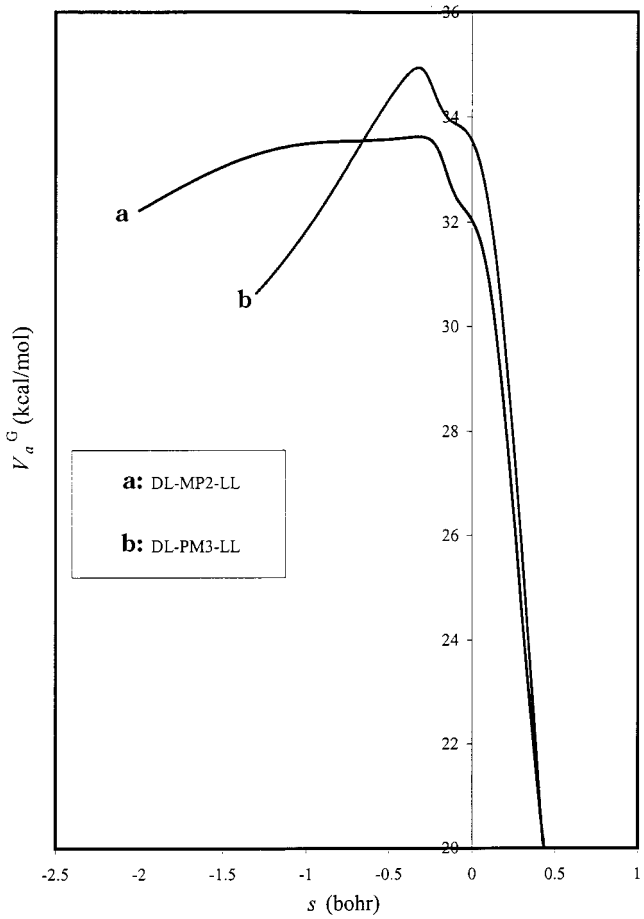

Figure 7. Dual-level vibrational adiabatic ground-state energy curves. Curves a and b are obtained using the MP2/6-31+G** (DL-MP2-LL) and PM3 (DL-PM3-LL) methods as the low-level calculation with classical barrier heights of 3.06 and 4.58 kcal/mol, respectively.

TABLE 6: Calculated Kinetic Isotope Effects (k_1/k_2) at Various Levels of Theory

	MP2/6-31+G*;[a] 2.80 kcal/mol[b]			MP2/6-31+G**;[a] 3.06 kcal/mol[b]		PM3;[a] 4.58 kcal/mol[b]	
T (K)	TST[c]	CVT	CVT/ μOMT	CVT	CVT/ μOMT	CVT	CVT/ μOMT
200	19.13	1.78	1.54	1.87	1.77	0.96	5.65
250	10.86	1.64	1.49	1.71	1.66	1.05	4.07
300	7.40	1.55	1.45	1.60	1.57	1.11	3.17
350	5.61	1.48	1.41	1.53	1.50	1.15	2.63
400	4.54	1.44	1.38	1.47	1.46	1.17	2.27
450	3.85	1.40	1.35	1.43	1.42	1.17	2.03
500	3.37	1.37	1.33	1.39	1.38	1.17	1.84
600	2.76	1.32	1.29	1.34	1.33	1.15	1.59
800	2.15	1.25	1.23	1.27	1.26	1.08	1.31
1000	1.87	1.21	1.19	1.22	1.21	1.03	1.18

[a] Low-level theory used in the dual-level VTST/MT calculation. [b] High-level classical barrier height used in the calculation. [c] KIEs calculated by high-level TST are independent of classical barrier heights and types of low-level calculation.

are 1.11 and 3.17, respectively. The calculated KIEs as a function of temperature by the high-level TST and the dual-level CVT/μOMT are plotted in Figure 8. The KIEs calculated by TST are highly temperature-dependent, changing from 19.1 at 200 K to 1.87 at 1000 K. The KIEs calculated by CVT/μOMT using MP2/6-31+G** as the low-level PES are not very sensitive to the temperature, changing from 1.77 at 200 K to 1.21 at 1000 K. On the other hand, the corresponding values using the PM3 method as the low-level PES show noticeable

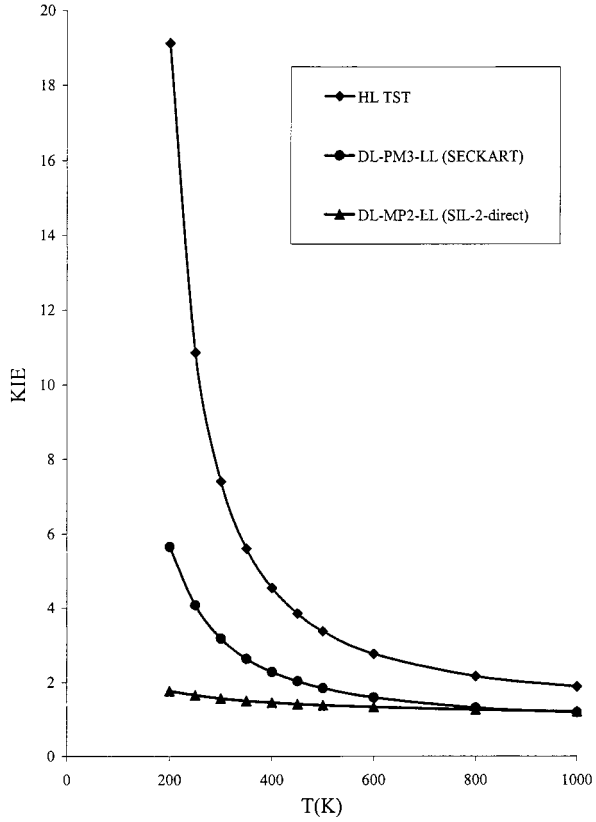

Figure 8. Temperature dependence of the calculated KIEs by high-level TST (HL-TST), dual-level CVT/μOMT with PM3 low-level and SECKART correction scheme (DL-PM3-LL), and dual-level CVT/μOMT with MP2/6-31+G** low-level and SIL-2-direct correction scheme (DL-MP2-LL) using 3.06 as the high-level classical barrier height.

TABLE 7: Factor[a] Analysis of the Calculated Kinetic Isotope Effects

		MP2/6-31+G**		PM3	
T (K)	$\eta_{vib}^{\ddagger}$	η_{var}[b]	$\eta_{tunneling}$[b]	η_{var}	$\eta_{tunneling}$
200	12.314	0.098	0.948	0.050	5.867
250	6.993	0.157	0.971	0.097	3.868
300	4.766	0.216	0.981	0.150	2.852
350	3.609	0.272	0.986	0.204	2.291
400	2.922	0.324	0.989	0.257	1.952
450	2.476	0.371	0.992	0.304	1.730
500	2.167	0.414	0.993	0.347	1.578
600	1.774	0.486	0.995	0.416	1.387
800	1.387	0.588	0.995	0.502	1.210
1000	1.206	0.651	0.995	0.549	1.149

[a] The translational and rotational contributions are independent of temperature and are 1.042 and 1.491, respectively. [b] Using 3.06 kcal/mol as the high-level classical barrier height

temperature dependence, changing from 5.65 at 200 K to 1.18 at 1000 K. In Table 7 the calculated KIEs by the CVT/μOMT method are broken into contributions from various factors,

$$\mathrm{KIE} = \eta_{trans}\eta_{rot}^{\ddagger}\eta_{vib}^{\ddagger}\eta_{var}\eta_{tunneling} \quad (5)$$

as described in several earlier studies.[29,48] As shown in Table 7, the rotational and vibrational contributions are responsible for the high KIEs calculated using TST, and the large temperature dependence comes solely from the vibrations. The variational effects, however, make a very strong inverse (<1.0) contribution to the KIEs at low temperatures, and result in much smaller KIEs and their temperature dependence by CVT. This

is because the variational effects are much more important in the hydrogen reaction (R1) than in the deuterated reaction (R2). The calculation using the PM3 method as the low-level PES showed even more inverse variational contribution. Interestingly, for the calculation using the MP2/6-31+G** theory as the low-level PES, the tunneling effects make slightly inverse contribution to the KIEs. This is, however, not unusual for a low-barrier reaction in which the deuterated reaction has a higher effective barrier to tunnel through.[48a] In the calculation using the PM3 method as the low-level PES, the barrier is higher and narrower, and thus the tunneling effects are more important in (R1) than in (R2) because the hydrogen tunnels more readily than the deuterium. Consequently, the tunneling effects make significant normal (>1.0) contribution to the KIEs at lower temperatures.

The above KIEs analysis suggests that experimental KIE study over a temperature range may be able to provide a clear test on the dynamical behaviors of the current reaction. If both variational and tunneling effects are small, the KIEs should be modeled correctly by the TST. Thus, very strong temperature dependence of KIEs and very high KIE values at low temperatures should be observed, as seen in Table 6 and Figure 8. On the other hand, if the tunneling effects are important, then the KIEs would be moderately temperature dependent and be significantly normal at or below room temperature, as in the calculation using the PM3 method as the low-level PES. The calculation using the more reliable MP2/6-31+G** method as the low-level PES suggests that only the variational effects are important, and the vibrational and variational contributions to the KIEs almost cancel each other out. If it is the case, than the observed KIEs would be slightly normal (1.5−1.6 at room temperature) and would show relatively small temperature dependence.

Concluding Remarks

It is worthwhile to compare the results of the current study to the similar OH + CH_4 system. Since the OH + CH_4 system is the prototype of the hydrogen abstraction reaction of hydrocarbons and halogenated hydrocarbons in the atmosphere, it has been extensively studied in recent years. However, recent more advanced theoretical studies seemed to raise more questions than they answered. First of all, there is significant uncertainty on the classical barrier height. For example, Vasilios and Truhlar[32] used the MP2/SAC method with an adjusted cc-pVTZ basis set and obtained a barrier of 7.4 kcal/mol. However, most of recent high-level calculations give lower values, e.g., 5.1 kcal/mol by Malick et al.[49] using the CBS-QCI-APNO method, 5.7 kcal/mol by Korchowiec et al.[50] by the G2M method, and 5.8 and 5.0 kcal/mol by Lluch et al.[51] using the CCSD(T)/aug-cc-pVTZ and CCSD(T)-SAC/cc-pVTZ methods, respectively. Also, earlier studies showed significant tunneling effects at low temperatures and very small variational effects.[28,32] However, recent experimental measurements indicated that the Arrhenius plot of the rate constants shows only slight curvature in the low-temperature range.[52] Furthermore, all recent VTST calculations showed significant variational effects.[13,23,51,53] On the other hand, the study by Vasilios and Truhlar[32] gave good agreement on the experimental rate constants and KIEs at most temperatures while recent VTST calculation[51,53] seemed to underestimate the deuterium KIEs (OH + CD_4), and in the TST study by Schwartz et al.[12] the KIEs were overestimated. In an ongoing project in our research group, we have calculated the classical barrier using QCISD(T) and CCSD(T) methods with 6-311++G(3df,3dp) basis set and the results are 6.1 and 6.3 kcal/mol, respectively. We have also applied the SIL-2 method employed in the current study to model the rate constants of the OH + CH_4 reaction. The preliminary results showed that the classical barrier is in the range 4.6−5.5 kcal/mol, and the variational effects also seemed important. The tunneling effects are, however, only slightly more important than the current system.

From the above, one can conclude that the dynamical behaviors of the OH + CH_4 reaction are far from being settled from the theoretical point of view. Since most of new calculation show 1−2 kcal/mol reduction of classical barrier than the value (7.4 kcal/mol) used by Vasilios and Truhlar,[32] the calculated rate constants would be much higher unless significant variational effects are also present. It might also be possible that the tunneling effects or the symmetry number ($\rho = 12$) was overestimated. However, the KIEs could be affected dramatically by the variational effects since in many cases the perprotic reactions show much larger variational effects than the perdeuterated ones. The variational effects are in fact very difficult to calculate accurately since they depend on the subtle details of the PES outside the stationary points. Furthermore, the choices of the hindered rotor treatment also have important effects on the calculated rate constants since the hindered rotor mode of the transition state is only about 40 cm^{-1}.

Experimentally, the OH + CH_3F rate constant is approximately three times larger than that of OH + CH_4 reaction at 300 K. From recent theoretical calculations, the true classical barrier of the current system is probably 1−2 kcal/mol lower than that of OH + CH_4 reaction. This is probably the main reason that the experimental rate constants show even smaller curvatures or tunneling effects. In both reactions, the tunneling contribution might not be as large as obtained in earlier theoretical studies.[12,13,28,32] Even though the general impression is that the hydrogen abstraction reactions would show large tunneling effects, however, when the energy barrier is wide, as in the present study, the tunneling may not be important. The lack of significant curvatures in the Arrhenius plots at low temperature is observed for many other hydrogen abstraction reactions of fluoro- and chloro-hydrocarbons.[7] The deuterium KIEs in the current system might be smaller than those in the OH + CH_4 reaction for the following reasons. First of all, the translational and rotational contributions to the KIEs, which are easily overlooked, are about 10% and 20% smaller in the current system, respectively, and these differences are independent of temperature. Furthermore, the tunneling contribution to the KIEs is probably smaller in the current system due to a lower barrier. The variational effects might play a more important role in the KIE differences since they contribute very inversely in the current study. However, the exact extent of variational contribution is difficult to evaluate since the variational effects differ significantly in VTST calculations using different PES.[13,22,28,32,51,53]

One might also be concerned whether the fitted classical barrier heights represent any physical reality since they are significantly lower than those obtained by most ab initio calculations. It is possible that the barrier was artificially fitted to compensate other errors. Within the validity of the VTST, the most likely sources of errors are the incorrect global features of the PES that determine the variational effects and the treatment of the hindered rotor. The latter is less likely to cause a lower barrier in the current study since the hindered rotor method used here gives very similar results to those using harmonic approximation. The harmonic approximation usually gives a partition function that is too high for the low-frequency modes above room temperature. If our treatment overestimated the partition function, then our fitted barriers are actually too

high. The possible overestimation of the variational effects, however, could lead to underestimation of the classical barrier. On the other hand, the best theoretical level we employed, QCISD(T)/6-311++G(3df,3pd), predicts a classical barrier of 4.4 kcal/mol, which is only 1.3−1.6 kcal/mol higher than the fitted values. It would not be very surprising that the current high-level ab initio theory cannot yet reach chemical accuracy for the classical barriers of a polyatomic reaction system involving a fluorine atom.

Summary

The thermal rate constants of the hydrogen abstraction reaction of fluoromethane (CH_3F) by the hydroxyl radical have been modeled by dual-level variational transition state theory including multidimensional tunneling calculation from 200 to 1000 K. The estimated classical barrier height is 2.8−3.1 kcal/mol, which is significantly lower than those by all previous theoretical studies. The calculated rate constants based on the estimated barriers are in very good agreement with recent experimental data at most temperatures. The calculation showed that the variational effects might be very important in the reaction while the tunneling effects are very small except at the lowest temperatures. The hydrogen kinetic isotope effects were predicted to be 1.5−1.6 at room temperature and to be only slightly temperature dependent. The KIE factor analysis showed that the strongly normal vibrational contribution is almost canceled out by the inverse variational contribution, and the rotational effect makes a significant contribution to the normal KIEs. The current study also showed that the KIEs are sensitive to the detailed features of the potential energy surface, and thus the experimental KIE study can be used, together with theoretical modeling, as a powerful tool to probe the nature of the PES for this type of chemical reactions.

Acknowledgment. This research is supported in part by the National Science Council of Taiwan, grant number NSC88-2113-M194-008. We thank Prof. Donald G. Truhlar of the Univeristy of Minnesota for providing the Gaussrate interface program. We are also grateful to the National Center for High-Performance Computing of Taiwan for providing the computational resources and technical support.

Supporting Information Available: Tables of calculated geometry, vibrational frequencies, rate constants, and parameters used in the SIL-2 scheme. This material is available free of charge via the Internet at http://pubs.acs.org.

References and Notes

(1) Wayne, R. P. In *Chemistry of Atmospheres*, 2nd ed.; Oxford Science Publication: Oxford, NY, 1991; p 160.

(2) (a) Giessing, A. M. B.; Feilberg, A.; Møgelberg, T. E.; Sehested, J.; Bilde, M.; Wallington, T. J.; Nielsen, O. J. *J. Phys. Chem.* **1996**, *100*, 6572. (b) Møgelberg, T. E.; Sehested, J.; Bilde, M.; Wallington, T. J.; Nielsen, O. J. *J. Phys. Chem.* **1996**, *100*, 8882. (c) Orkin, V. L.; Huie, R. E.; Kurylo, M. J. *J. Phys. Chem.* **1996**, *100*, 8907. (d) Wallington, T. J.; Hurley, M. D.; Fracheboud, J. M.; Orlando, J. J.; Tyndall, G. S.; Sehested, J.; Møgelberg, T. E.; Nielsen, O. J. *J. Phys. Chem.* **1996**, *100*, 18116. (e) Chen, J.; Young, V.; Niki, H.; Magid, H. *J. Phys. Chem. A* **1997**, *101*, 2648. (f) Møgelberg, T. E.; Sehested, J.; Tyndall, G. S.; Orlando, J. J.; Fracheboud, J.-M.; Wallington, T. J. *J. Phys. Chem. A* **1997,** *101*, 2828. (g) Louis, F.; Talhaoui, A.; Sawerysyn, J.-P.; Rayez, M.-T.; Rayez, J.-C. *J. Phys. Chem. A* **1997,** *101*, 8503. (h) Orkin, V. L.; Huie, R. E.; Kurylo, M. J. *J. Phys. Chem. A* **1997**, *101*, 9118. (i) DeMore, W. B.; Wilson, E. W., Jr. *J. Phys. Chem. A* **1999,** *103*, 573. (j) Yamada, T.; Fang, T. D.; Taylor, P. H.; Berry, R. J. *J. Phys. Chem. A* **2000,** *104*, 5013.

(3) Sandorfy, C. *Atmos. Environ.* **1976**, *10*, 343 and references therein.

(4) Howard, C. J.; Evenson, K. M. *J. Chem. Phys.* **1976**, *64*, 197.

(5) Nip, W. S.; Singleton, D. L.; Overend, R.; Paraskevopoulos, G. *J. Phys. Chem.* **1979**, *83*, 2440.

(6) (a) Jeong, K. M.; Kaufman, F. *J. Phys. Chem.* **1982**, *86*, 1808. (b) Jeong, K. M.; Kaufman, F. *J. Phys. Chem.* **1982**, *86*, 1816.

(7) (a) Atkinson, R. *Chem. Rev.* **1985**, *85*, 69. (b) Atkinson, R. *J. Phy. Chem. Ref. Data* **1989**, Monograph No 1.

(8) (a) Cohen, N.; Benson, S. W.*J. Phys. Chem.* **1987**, *91*, 162. (b) Cohen, N.; Benson, S. W. *J. Phys. Chem.* **1987**, *91*, 171.

(9) Schmoltner, A. M.; Talukdar, R. K.; Warren, R. F.; Mellouki, A.; Goldfarb, L.; Gierczak, T.; Mckeen, S. A.; Ravishankara, A. R. *J. Phys. Chem.* **1993**, *97*, 8976.

(10) Hsu, K. J.; DeMore, W. B. *J. Phys. Chem.* **1995**, *99*, 1235.

(11) DeMore, W. B. *J. Phys. Chem.* **1996**, *100*, 5813.

(12) Schwartz, M.; Marshall. P.; Berry, R. J.; Ehlers, C. J.; Petersson, G. A. *J. Phys. Chem. A* **1998**, *102*, 10074.

(13) Espinosa-García, J.; Coitiño, E. L.; González, A.; Lluch, J. M. *J. Phys. Chem. A* **1998**, *102*, 10715.

(14) Eyring, H. *J. Chem. Phys.* **1935**, *3*, 105.

(15) Truhlar, D. G.; Garrett, B. C. *Acc. Chem. Res.* **1980,** *13*, 440.

(16) Wigner, E. P. *Z. Phys. Chem. Abt. B* **1932**, *19*, 203.

(17) Truhlar, D. G.; Isaacson, A. D.; Garrett, B. C. In *The Theory of Chemical Reaction Dynamics*; Baer, M., Ed.; CRC Press: Boca Raton, FL, 1985; Vol. 4, p 65.

(18) Eckart, C. *Phys. Rev.* **1930**, *35*, 1303.

(19) Corchado, J. C.; Espinosa-García, J.; Roberto-Neto, O.; Chuang, Y.-Y.; Truhlar, D. G. *J. Phys. Chem. A* **1998**, *102*, 4899.

(20) Corchado, J. C.; Truhlar, D. G.; Espinosa-García, J. *J. Chem. Phys.* **2000**, *112*, 9375.

(21) Roberto-Neto, Orlando; Coitiño, E. L.; Truhlar, D. G. *J. Phys. Chem. A* **1998**, *102*, 4568.

(22) Kim, Y.; Corchado, J. C.; Villà, J.; Xing, J.; Truhlar, D. G. *J. Chem. Phys.* **2000,** *112*, 2718.

(23) Huang, C.-H.; You, R.-M.; Lian, P.-Y.; Hu, W.-P. *J. Phys. Chem. A* **2000**, *104*, 7200.

(24) Garrett, B. C.; Joseph, T.; Truong, T. N.; Truhlar, D. G. *Chem. Phys.* **1989**, *136*, 271.

(25) (a) Liu, Y.-P.; Lynch, G. C.; Truong, T. N.; Lu, D.-H.; Truhlar, D. G.; Garrett, B. C. *J. Am Chem. Soc.* **1993**, *115*, 2408. (b) Lu, D.-h.; Truong, T. N.; Melissas, V. S.; Lynch, G. C.; Liu, Y.-P.; Garrett, B. C.; Steckler, R.; Isaacson, A. D.; Rai, S. N.; Hancock, G. C.; Lauderdale, J. G.; Joseph, T.; Truhlar, D. G. *Comput. Phys. Commun.* **1992**, *71*, 235.

(26) Liu, Y.-P.; Lu, D.-H.; Gonzalez-Lafont, A.; Truhlar, D. G.; Garrett, B. C. *J. Am Chem. Soc.* **1993**, *115*, 7806.

(27) Truong, T. N.; Lu, D.-h.; Lynch, G. C.; Liu, Y.-P.; Melissas, V. S.; Stewart, J. J. P.; Steckler, R.; Garrett, B. C.; Isaacson, A. D.; González-Lafont, A.; Rai, S. N.; Hancock, G. C.; Joseph, T.; Truhlar, D. G. *Comput. Phys. Commun.* **1993**, *75*, 143.

(28) Hu, W.-P.; Liu, Y.-P.; Truhlar, D. G.*J. Chem. Soc., Faraday Trans.* **1994**, *90*, 1715.

(29) Corchado, J. C.; Espinosa-García, Joaquin; Hu, W.-P.; Rossi, I.; Truhlar, D. G. *J. Phys. Chem.* **1995**, *99*, 687.

(30) Hu, W.-P.; Rossi, I.; Corchado, J. C.; Truhlar, D. G. *J. Phys. Chem. A* **1997**, *101*, 6911.

(31) (a) Villà, J.; Gonzalez-Lafont, A.; Lluch, J. M.; Truhlar, D. G. *J. Am. Chem. Soc.* **1998**, *120*, 5559. (b) Villà, J.; Corchado, J. C.; González-Lafont, A.; Lluch, J. M.; Truhlar, D. G. *J. Phys. Chem. A* **1999**, *103*, 5061.

(32) (a) Melissas, V. S.; Truhlar, D. G. *J. Chem. Phys.* **1993**, *99*, 1013. (b) Melissas, V. S.; Truhlar, D. G. *J. Chem. Phys.* **1993**, *99*, 3542. (c) Melissas, V. S.; Truhlar, D. G. *J. Phys. Chem. A* **1994**, *98*, 875.

(33) Stewart, J. J. P. *J. Comput. Chem.* **1989**, *10*, 209, 221.

(34) (a) Dewar, M. J. S.; Zoebisch, E. G.; Healy, E. F.; Stewart, J. J. P. *J. Am. Chem. Soc.* **1985**, *107*, 3902. (b) Dewar, M. J. S.; Zoebisch, E. G. *J. Mol. Struct. (THEOCHEM)* **1988**, *180*, 1.

(35) Hehre, W. J.; Radom, L.; Schleyer, P. V. R.; Pople, J. A. *Ab initio Molecular Orbital Theory*; John Wiley & Sons: New York, 1986.

(36) Frisch, M. J.; Trucks, G. W.; Schlegel, H. B.; Scuseria, G. E.; Robb, M. A.; Cheeseman, J. R.; Zakrzewski, V. G.; Montgomery, J. A., Jr.; Stratmann, R. E.; Burant, J. C.; Dapprich, S.; Millam, J. M.; Daniels, A. D.; Kudin, K. N.; Strain, M. C.; Farkas, O.; Tomasi, J.; Barone, V.; Cossi, M.; Cammi, R.; Mennucci, B.; Pomelli, C.; Adamos, C.; Clifford, S.; Ochterski, J.; Petersson, G. A.; Ayala, P. Y.; Cui, Q.; Morokuma, K.; Malick, D. K.; Rabuck, A. D.; Raghavachari, K.; Foresman, J. B.; Cioslowski, J.; Ortiz, J. V.; Baboul, A. G.; Stefanov, B. B.; Liu, G.; Liashenko, A.; Piskorz, P.; Komaromi, I.; Gomperts, R.; Martin, R. L.; Fox, D. J.; Keith, T.; Al-Laham, M. A.; Peng, C. Y.; Nanayakkara, A.; Gonzalez, C.; Challacombe, M.; Gill, P. M. W.; Johnson, B. G.; Chen, W.; Wong, M. W.; Andres, J. L.; Head-Gordon, M.; Replogle, E. S.; Pople, J. A. *Gaussian 98*, Revision A.7; Gaussian, Inc.: Pittsburgh, PA, 1998.

(37) Møller, C.; Plesset, M. S. *Phys. Rev.* **1934**, *46*, 618.

(38) Pople, J. A.; Head-Gordon, M.; Raghavachari, K. *J. Chem. Phys.* **1987**, *87*, 5968.

(39) (a) Page, M.; McIver, J. W., Jr. *J. Chem. Phys.* **1988**, *88*, 922. (b) Page, M.; Doubleday: C.; McIver, J. W., Jr. *J. Chem. Phys.* **1990**, *93*, 5634.

(40) (a) Chuang, Y.-Y.; Truhlar, D. G. *J. Phys. Chem. A* **1998**, *102*, 242. (b) Chuang, Y.-Y.; Truhlar, D. G. *J. Chem. Phys.* **1997**, *107*, 83.

(41) Lias, S. G.; Bartmess, J. E.; Liebman, J. F.; Holmes, J. L.; Levin, R. D.; Mallard, W. G. *J. Phys. Chem. Ref. Data* **1988,** *17*, Suppl. 1.

(42) Chuang, Y.-Y.; Truhlar, D. G. *J. Chem. Phys.* **2000**, *112*, 1221.

(43) Chuang, Y.-Y.; Truhlar, D. G. *J. Phys. Chem. A* **1997**, *101*, 3808.

(44) Melissas, V. S.; Truhlar, D. G.; Garrett, B. C. *J. Chem. Phys.* **1992**, *96*, 5758.

(45) Corchado, J. C.; Chuang, Y.-Y.; Coitiño, E. L.; Truhlar, D. G. *Gaussrate*, version 8.2. University of Minnesota, 1999.

(46) Chuang, Y.-Y.; Corchado, J. C.; Fast, P. L.; Villà, J.; Hu, W.-P.; Liu, Y.-P.; Lynch, G. C.; Nguyen, K. A.; Jackels, C. F.; Gu, M. Z.; Rossi, I.; Coitiño, E. L.; Clayton, S.; Melissas, V. S.; Steckler, R.; Garrett, B. C.; Isaacson, A. D.; Truhlar, D. G. *Polyrate*, version 8.2. University of Minnesota, 1999.

(47) Chase, M. W.; Jr.; Davies, C. A.; Downey, J. R., Jr.; Frurip, D. J.; McDonald, R. A.; Syverud, A. N. *J. Phys. Chem. Ref. Data* **1985**, *14*, Suppl. 1.

(48) (a) Wu, Y.-R.; Hu, W.-P. *J. Am. Chem. Soc.* **1999**, *121*, 10168. (b) Hu, W.-P.; Truhlar, D. G. *J. Am. Chem. Soc.* **1996**, *118*, 860. (c) Zhao, X. G.; Tucker, S. C.; Truhlar, D. G. *J. Am. Chem. Soc.* **1991**, *113*, 826. (d) Hu, W.-P.; Truhlar, D. G. *J. Am. Chem. Soc.* **1994**, *116*, 7797. (e) González-Lafont, A.; Truong, T. N.; Truhlar, D. G. *J. Phys. Chem.* **1991**, *95*, 4618.

(49) Malick, D. K.; Peterson, G. A.; Montgomery, J. A., Jr. *J. Chem. Phys.* **1998**, *108*, 5704.

(50) Korchowiec, J.; Kawahara, S.-i.; Matsumura, K.; Uchimaru, T.; Sugie, M. *J. Phys. Chem. A* **1999**, *103*, 3548.

(51) Masgrau, L.; González-Lafont, A.; Lluch, J. M. *J. Chem. Phys.* **2001**, *114*, 2154.

(52) Gierczak, T.; Talukdar, R. K.; Herndon, S. C.; Vaghjiani, G. L.; Ravishankara, A. R. *J. Phys. Chem. A* **1997**, *101*, 3125.

(53) Espinosa-García, J.; Corchado, J. C. *J. Chem. Phys.* **2000**, *112*, 5731.